This article has been published in Int Endod J. 2018 Feb 28. doi: 10.1111/iej.12918

Title: Ions-modified nanoparticles induce different apatite formations at cervical dentin.

Authors: Manuel Toledano[a], Manuel Toledano-Osorio[a], Antonio Luis Medina-Castillo[b], Modesto T. López-López[c], Fátima S. Aguilera[a*], Raquel Osorio[a].

Institution: [a]University of Granada, Faculty of Dentistry, Dental Materials Section.
Colegio Máximo de Cartuja s/n
18071 – Granada - Spain.
[b]University of Granada, NanoMyP. Spin-Off Enterprise.
Edificio BIC-Granada. Av. Innovación 1.
18016 - Armilla, Granada, Spain.
[c]University of Granada, Faculty of Science, Applied Physics Department.
Av. Fuente Nueva s/ n 18071 Granada - Spain.

Running title: New mineral at cervical dentin

Keywords: Dentin, hypersensitivity, microscopy, remineralization, TEM, XRD.

***Corresponding author:** Prof. Fátima S. Aguilera
Dental Materials Section
University of Granada, Faculty of Dentistry
Colegio Máximo de Cartuja s/n
18071 – Granada - Spain.
Tel.: +34-958249797
Fax: +34-958240809
Email: fatimas@ugr.es

Abstract

Aim: The aim of this research was to investigate if mineral and ultrastructure is modified when cervical dentin is treated with four different nanogels-based solutions for remineralizing purposes. **Methodology**: Experimental nanogels based on zinc, calcium and doxycycline-loaded polymeric nanoparticles were applied on citric acid etched dentin to facilitate the occlusion of tubules and the mineralization of the dentin surface. Dentin surfaces were studied by X-ray diffraction and transmission electron microscopy through selected area diffraction and bright-field imaging and selected area electron diffraction. **Results:** Crystals at the dentin surface were identified as hydroxyapatite with the highest crystallographic maturity and crystallite size in dentin treated with Zn-NPs based-gel. Texture increased in all samples from 24 h to 7 d, except in dentin surfaces treated with Zn-NPs gel. Polyhedral, plate-like and drop-like shaped apatite crystals constituted the bulk of minerals in dentin treated with Zn-NPs gel, after 7 d. Polymorphic, cubic and needle-like shaped crystals characterized minerals, more amorphous in dentin treated with Ca-NPs gel after 7 d than that found when Zn-NPs were applied. Doxycycline-NPs produced the smallest crystallites with poor crystallinity, maturity and chemical stability. **Conclusions:** Crystalline and amorphous phases of hydroxyapatite, described in both type of dentin treated with Zn-NPs as well as Ca-NPs gels, delayed the effect of erosion and contribute to improve the biomedical properties of cervical dentin after remineralization. Doxycycline-NPs based-gel are not recommended to treat dentin hypersensitivity.

Introduction

Dentin is a mineralized connective tissue that constitutes the bulk of the tooth. It is composed of a continuous network of type I collagen fibrils and mineral. Each mineralized fibril is a composite of a collagen framework and very thin needle- and plate-shaped crystals of apatite crystallites (48%). The size of the biological apatite crystals in dentin is roughly 5 x 30 x 100 nm, they have less calcium than stoichiometric HAp and contains 4-5% carbonate. Lower calcium content and higher carbonate content make HAp vulnerable to acids attack (Zavgorodniy *et al.* 2008). Thereby, this nanostructure may affect dentin tissue regeneration with direct clinical implications.

Dentin hypersensitivity (DH) is an oral health problem in adults on a global scale. DH is clinically described as a non-spontaneous, localized, intense pain of short duration that ceases when stimuli are removed. Erosion plus demineralization has been considered the main etiological factor for DH, because of the opening and enlarging of the dentin tubules (Yoshizaki *et al.* 2017). Several desensitizing products including varnishes, resins and remineralizing agents have been proposed to provide tubule occlusion trying to treat DH, but with uncertain results (Wang *et al.* 2011, Peumans *et al.* 2014). Nanogels are 100-nm globular particles synthesized through a versatile route with methacrylate functionalization. Dentin infiltration with these polymeric nanoparticles as calcium and phosphate sequestering materials has been previously proposed (Osorio *et al.* 2016a). These polymers bind to collagen and facilitate amorphous calcium-phosphate precursor formations. Nanopolymers may act as carriers of other biological factors for the management of tissue mineralization, as zinc, calcium (Toledano *et al.* 2017) and doxycycline. Doxycycline promotes the release of osteogenic factors such as the transforming growth factor, insulin-like growth factor, or the bone morphogenetic proteins that trigger hard tissue induction (Chaturvedi *et al.* 2008).

The dimensions and morphology of the formed HAp crystals affect its mechanical properties (Wang *et al.* 2010) and may predetermine its clinical service. X-ray diffraction (XRD) is one of the most powerful techniques to study the hierarchical structure of biological mineral such as teeth and bone. Thus, analytical and morphological data may be obtained in the same sample, as HAp is going to be assessed peak-to-peak approach using the Scherrer formulae. Transmission electron microscopy (TEM) and selected area electron diffraction pattern (SAED) have been employed to characterize the

size, shape and nanostructures. The purpose of the present study was to elucidate if the crystallinity and amorphization of cervical dentin is influenced by the treatment with four different nanogels-based solutions for remineralizing purposes. The null hypothesis is that there are no differences in crystal morphology, structure and texture of cervical dentin treated with four different nanogels-based solutions.

Materials and Methods

Nanoparticles production

PolymP-*n* Active nanoparticles (NPs) (NanoMyP, Granada, Spain), fabricated trough polymerization precipitation, were purchased (Medina-Castillo *et al.* 2010). NPs are composed by 2-hydroxyethyl methacrylate (backbone monomer), ethylene glycol dimethacrylate (cross-linker) and methacrylic acid (functional monomer). Calcium-doped NPs and Zinc-doped NPs were produced. For zinc and calcium complexation 30 mg of NPs were immersed at room temperature, during 3 days under continuous shaking in 15 ml aqueous solutions of $ZnCl_2$ or $CaCl_2$ (containing zinc or calcium at 40 ppm at pH 6.5), in order to reach the adsorption equilibrium of metal ions. Then, the suspensions were centrifuged and the particles were separated from the supernatant. Attained ion complexation values are 0.96 ± 0.04 µg Ca/mg NPs and 2.15 ± 0.05 µg Zn/mg NPs (Osorio *et al.* 2016b). A third group of NPs doped with doxycycline hyclate was introduced in the study. 30 mg of NPs were immersed in 18 ml of 40 mg/ml aqueous solution of doxycycline hyclate (Sigma Aldrich, ChemieGmbh, Riedstr, Germany), during 4 hours, under continuous shaking. Then, the suspensions were centrifuged and the particles were separated from the supernatant. Four different NPs were tested: 1) NPs (NPs), 2) NPs doped with Ca (Ca-NPs), 3) NPs doped with Zn (Zn-NPs), and 4) NPs doped with doxycycline hyclate (D-NPs).

Specimens preparation

15 sound, single-rooted teeth were obtained with informed consent from donors (18 to 25 yr of age), under a protocol approved by the Institution review board (405/CEIH/2017). Two dentin blocks from the buccal surface of each root, just below the cementodentinal junction were obtained by cutting with a diamond saw (Accutom-50 Struers, Copenhagen, Denmark) under copious water irrigation. The surfaces were polished through SiC abrasive papers from 800 up to 4000 grit followed by final polishing steps performed using diamond pastes through 1 µm down to 0.25 µm (Struers LaboPol-4; Struers

GmbH, Hannover, Germany) (Fig. S2). Specimens were prescreened for tubule occlusion with AFM and those with occluded tubules were excluded (Saeki *et al.* 2016).

Dentin samples were dipped into a citric acid solution (pH 3.8) for 1 min to ensure the patency of the dentinal tubules and remove the smear layer. Dentin surfaces were washed and ultrasound treated for 10 min before NPs application. A phosphate buffer saline (PBS) suspension of NPs, Zn-NPs, Ca-NPs, D-NPs (10 mg/ml) or just a PBS solution were applied (30 s), in each of the five different experimental groups. Specimens were stored in PBS at 37º C for 24 hours and 7 days.

X-Ray Diffraction (XRD) analysis

Treated surfaces were submitted to XRD analysis. The X-ray micro-diffractometer (μXRD^2) used in this study was a single crystal diffractometer with a 2-dimensional detector system Cmos Photon 100 (Bruker-D8 Venture, Wien, Austria), equipped with kappa geometry based goniometer 2D Detector and XRD 2D Scan software. The X-ray beam (Cu Kα line, λ = 1.5418 Å) was generated by a Cu Microforms source Iμs and generator settings of 50.00 kV/1.00 mA were employed. The 2D position sensitive detector had 1024x1024 pixels. Both the starting and ending positions were: distance, 40.00 mm; 2θ: 40.00°; Omega: 20.00°; Phi: 270.00°; Chi: 50.00°. Wavelength of 1.54184 Å (Cu). The sample to detector distance was 40.00 mm, 2θ scanning angle range was from 10° to 80°. All measurements were performed at room temperature (295±0.1°K) and an exposure time of 60.00 s. A voltage of 50.00 kV, a current of 1.000 mA with the anode of Cu were used for the generator. The rest of the procedure is as in Toledano *et al.* (2016).

From the X-ray micro-diffraction pattern, the size and the preferred orientation of the crystallites were calculated (Perales *et al.* 2008, Xue *et al.* 2013):

$$d = \frac{K\lambda}{\beta \cos\theta} \qquad (1)$$

In this equation d is the mean size of the crystallites, K is a dimensionless shape factor, with a value close to unite –note that in the case of dentin, $K \approx 0.94$ (Xue *et al.* 2013), and β is the peak full width at half maximum (FWHM) of the line broadening. In order to obtain the crystallite length and width,

this formula was used for the line broadenings corresponding to 002 (*H*) and 310 (*L*) reflections, respectively (see data in Table 1). In order to determine the interaction of variables with the HAp structure the ratio *H/L* (Bigi *et al.* 2004) was also measured. The preferred orientation of the crystallites (texture) from the following intensity ratios (Xue *et al.* 2013):

$$R_{hkl} = k_{hkl} \frac{I_{211}}{I_{hkl}} \qquad (2)$$

In this expression I_{211} and I_{hkl} are the intensities corresponding respectively to line reflections 211 and *hkl*, and $k_{hkl} = \frac{I^{st}_{hkl}}{I^{st}_{211}}$,

where the superscript *st* refers to intensities calculated according to the JCPDS card (Low 2004, Xue *et al.* 2013).

Transmission Electron Microscopy (TEM) analysis

Dentin samples were crushed into a fine-grained powder in a liquid nitrogen mortar and pestle, and 2% NaOCl was added to remove the surrounding collagen, with daily changes for a week (using a sonicator). After washing with H_2O and ethanol, the nanocrystals were transferred to a 3 mm diameter carbon/Formvar coated cooper TEM grid (Toledano *et al.* 2016). Before analysis, all samples were sputter coated with a thin layer of amorphous carbon. Electron lucent particles were selected by size and distant from grid bars. Stack images were acquired, and the position of the stage was changed between -40 and +50° of α tilt, and collected every 10º. The samples were analyzed using a Transmission Electron Microscope Zeiss Libra 120 (Oberkochen, Germany) at 120 kV in bright-field (BF), and selected area electron diffraction (SAED) patterns were also captured. Normal BF images were produced by tilting the beam to the diffracting plane of interest. Tomographic reconstructions and related data were proceeded with the software iTEM (Olympus Soft Imaging Solutions GmbH, Münster, Germany), comprising acquisition, alignment and visualization. A specific semi-automated modulus for image processing, attached to the microscope, including a 2048x2048 pixel chip BM-2k-120 Dual-Speed on axis SSCCD-camera (TRS, Moorenweis, Germany), was used. Rough images alignment was undertaken on a neighboring crystal, in order to minimize radiation damage. The

obtained images were aligned and back projected using the software for 3D from the iTEM tomography extension. Reconstructions were obtained with a silicon graphics workstation self-incorporated.

Results

Micro-X-ray diffraction pattern

The analysis of μXRD^2 profiles of cervical dentin showed that the physical broadening (FWHM) of peaks at 002 (2θ, 25.900º; centroid peak position θ_{hkl}, 0/0/-2; I, 10977386) reflection, after observing *data* plotted by the reduced full width and extended height at half maximum of the phosphate band, was lower (~1.2 fold) in dentin surfaces treated with Zn-NPs based-gel when compared with the untreated group, after 7 d of PBS storage. Similarly, after 7 days, peaks at 310 (2θ, 40.127º; centroid peak position θ_{hkl}, -3/1/0; I, 1380390) showed FWHM values ~1.1 fold lower on dentin treated with Zn-NPs based-gel than those attained at the untreated dentin group (Table 1).

When dentin was treated with Zn-NPs, after observing the reflection at 211 peak and the diffraction ring corresponding to 211 and 112 planes (Fig. 1, inset b), it may be noted higher crystallinity values after 7 d of storage than those obtained after 24 h (Fig. 1, inset a). This crystallinity was also higher than in the untreated group after 7 d (Fig. 1, inset c). The analysis of μXRD^2 profiles confirmed high intensity of HAp after 7 d of storage at 002, 210, 211 and 112 peaks (Fig. 2, red bars). FWHM decreased in cervical dentin treated with Ca-NPs based-gel from 24 h to 7 d of storage. After 7 d, FWHM values at Ca-NPs treated dentin was ~1.2 fold lower than those obtained for the untreated group (Table 1) (Fig. 2). Minerals at the dentin surface treated with D-NPs based-gel showed the lowest crystallinity at 7 d storage (Table 1).

Crystalline size assessment

A qualitative estimation of the size of the coherently scattering domain (*i.e.* the crystallite size) is reported in Table 1. The shortest [τ_{002} (H)] (9.45 nm) and narrowest [τ_{310} (L)] (4.7 nm) crystallite size corresponded to dentin treated with D-NPs based-gel 7 d (Table 1). The ultra-structural observations at 002 reflections of treated cervical dentin confirmed that the grain size, expressed throughout the Scherrer-Wilson equation (Eq. 2) of dentin crystals became smaller in D-NPs, 7 d (9.21 nm). In the group of dentin treated with Zn-NPs, the dentin crystals attained the highest grain size (10.54 nm) (Table

1). On the contrary, at 310 reflections, the maximum grain size was achieved in dentin treated with the undoped-NPs based-gel.

Texture assessment

Texture indices (R_{hkl}) in dentin polycrystalline structures were calculated according to Eq. (2). At 002 plane, the texture assessed at the cervical dentin treated with all nanogels followed the trend: D-NPs < Zn-NP < Ca-NPs = undoped-NPs based-gels (Table 1).

Transmission electron microscopy (TEM) analysis

After 7 d, the cervical dentin that was treated with Zn-NPs based-gel exhibited, in bright-field (BF), distinct morphologies as polymorph/polyhedral (Fig. 3a), staggered block-like crystallites (Fig. 3f) or drop- plate-like crystals (Fig. 3h). They were transparent enough to observe their lattice, and also stable enough for tilt series acquisition (Figs. 3a, 3b, 3c, 3d). The polymorph/polyhedral crystals (Fig. 3a) were confirmed to be more amorphous in nature than that rounded in plate morphologies (Figs. 3f, 3g), as was observed from the diffuse ring pattern (Fig. 3e, inset). The predominant ring pattern corresponding to 002 planes appeared in form of two semi-circles (Figs. 3g, 3k, 3l). Ca-NPs based-gel applied in dentin samples and observed after TEM analysis, created characteristics polymorphic crystallites, platy needle shaped (Figs. 4d, 4e, 4f), cubic (Fig. 4f) or with staggered order (Fig. 4h). The predominant ring pattern corresponding to 002 planes appeared in form of two semi-circles (Fig. 4i). Diffuse halo rings were observed at dentin surface treated with D-NPs (Fig. S3d) and untreated dentin (Fig. S4d).

Discussion

Crystallites, with improved crystallographic orientation, became shorter and thinner in cervical dentin treated with Zn-NPs based-gel, thus contributing to enhance the mechanical strength of the dentin and providing a local ions-rich environment for further remineralization.

Considering the dentin treated with Zn-NPs, a full width half maximum (FWHM) decrease was observable (~1 fold) when data from specimens stored 7 d were compared to 24 h (Table 1) (Fig. 1). These high and sharp peaks or peak broadening (Zhang *et al.* 2003) parallel to the *c*-axes (Hanschin & Stern 1995) [002 plane] in the μXRD^2 (Table 1), indicated that cervical dentin at 7 d storage has less amorphous HAp (Moshaverinia *et al.* 2008) than that stored for 24 h. This HAp has also less crystals

imperfections in nanocrystallite materials, *i.e.,* it has great crystallite size and lattice distortion (Zhang *et al.* 2003). In general, the narrower the spectral peak width is, the higher the degree of mineral crystallinity (Karan *et al.* 2009), *i.e*., a perfect crystal would extend in all directions to infinity. Diffractography patterns gradually transform from broad diffuse peaks at cervical dentin treated with Zn-NPs based-gel (24 h or untreated 7 d), to sharper and more crystalline peaks after 7 d (Fig. 1). This confirm that amorphous phase itself is dynamic in nature. Similarly, at Zn-NPs treated dentin, the diffraction analysis formed brighter rings after 7 d (Fig 1, inset b) at 002, 211 and 112 planes, if compared with the 24 h time point (Fig. 1, inset a), indicating low line broadening of peaks. From findings of selected area electron diffraction (SAED) at an assembly of crystal polygons from figure 3i is clearly observed that the mineral phase, at this specific location, is crystalline HAp (Gajjeraman *et al*. 2007). On the other hand, the diffuse ring observed at SAED (Fig 3e, inset) when dentin was treated with Zn-NPs indicated decrease crystallinity (Wang *et al.* 2010), probably amorphous calcium phosphate or octocalcium phosphate (Bodier-Houllé *et al.* 1998). After 7 d, the faint preferred orientation (R_{hkl}) that was observed (Table 1) when cervical dentin was treated with Zn-NPs based-gel, (1.263) if compared with samples treated with Ca-NPs based-gel (1.599) might suggest that these apatite crystallites formed in the presence of zinc precipitated without any associated biologically controlled mineralization process (Zavgorodniy *et al.* 2008).

Dentin treated with Ca-NPs based-gel showed a brighter ring at 002 plane at 7 d than at 24 h; it means high HAp intensity (~$2x10^2$ counts less) (Fig. 2), and high crystallinity in both 002 and 310 planes (Table 1). The FWHM increase obtained after treating surfaces with Ca-NPs for 7 d and compared with that at 24 h, indicated a crystallinity increase. When this FWHM was compared with dentin treated with Zn-NPs based-gel at 7 d, there were physical broadening at both 002 and 310 planes (Table 1). The resulted broadening suggests the state of HAp as ultrafine nano-crystalline (Liu *et al*. 2013). Generally, the HAp with lower crystallinity found in dentin treated with Ca-NPs based-gel has the best bioactivity, biocomopatibility and biodegradability as compared with the stoichiometric HAp.

The crystallite size, derived from Eqs. (1) and (2), is regarded as the size of the coherently diffracting domains and it is not necessarily the same as apatite particle size (Bindu & Thomas 2014). After 7 d, mean crystallite size along a direction parallel and perpendicular to the *c*-axis [τ_{002} (*H*)] and

[τ_{310} (L)] of the dentin treated with Zn-NPs was ~1.2 fold higher than those of untreated dentin, and ~1.0 fold higher if compared with dentin treated with Ca-NPs based-gel. This expansion of the *c*-axis occurs by the substitution of the planar CO_3 group for the larger tetrahedral PO_4 group, and the opposite effect occurs when the OH group is substituted. Apart from that, H/L ratio increased in dentin treated with Zn-NPs more than in the rest of the groups (Table 1). This finding suggests a strong interaction of Zn-NPs with the HAp structure (Bigi *et al.* 2004). Cervical dentin treated with D-NPs created, after 7 d storage, HAp with the lesser needle shaped (decreased in average length) (Fig. S3a), probably related to the incorporation of carbonate as substituent for PO_4^{-3} in the apatite lattice (Hanschin & Stern 1995, Toledano *et al.* 2017). TEM pictures of dentin treated with D-NPs exhibited block-like apatite crystals (Fig. S3a) of 9.45 and 4.73 nm at 002 and 310 reflections, respectively (Table 1). The association of both values, *i*.e, FWHM and crystallite size led to an amorphization process (Lee *et al.* 2013).

Texture is the distribution of crystallographic orientation of a polycrystalline sample. It accounts for changes in microstructure, proving a great influence on materials properties, as cracking resistance (Liss *et al.* 2003). For $R \approx 1$, the grains were considered randomly oriented (Xue *et al.* 2013). The closest group to this criterion after 7 d of storage was the D-NPs based-gel, (R_{hkl}= 1.102) (Table 1). Cervical dentin treated with both Ca-NPs and undoped-NPs based-gels showed slightly distinct textures (Liss *et al.* 2003). Nevertheless, TEM analysis of dentin treated with Ca-NPs based-gel reveals, in PBS, that crystals are composed of domains of locally oriented crystal arrays, showing a well-defined lineation (Figs. 4d, 4e, 4f), of submicron size crystals (Fig. 4i). This also indicates that the TEM data trend is consistent with the referenced XRD data. *R* values greater or lower than 1.0 correlates with the presence of preferred grain orientation or texture (Low 2004), in a given (*hkl*) direction (Bindu & Thomas 2014). Values $0<R_{hkl}<1$ denote the lack of grains oriented in that direction (Bindu & Thomas 2014). The predominant ring pattern corresponding to 002 planes appearing in form of two semi-circles instead of a continuous ring, when Zn-NPs were 7 d applied (Figs. 3g, 3k, 3l), show that the crystallites have preferred orientation in *c*-direction (Landau & Lifshit 1980). As a result, dentin surfaces treated with Zn-NPs based-gel have the tendency toward random orientation over time, at 002 plane, as it represented the only group that decreased its R_{hkl} from 24 h (1.402) to 7 d (1.263) evaluation (Table 1), attaining negative nano-degradation (Low 2004). The wide variation of *R* values within both reflection

modes (002 and 310) suggests the existence of a strong gradation in texture at the nanometer scale within the complex dentin microstructure. Therefore, the null hypothesis that there are no differences in crystal morphology, structure and texture of cervical dentin treated with four different nanogels-based solutions, must be rejected.

These are, to the best of our knowledge, the only available results from both μXRD[2] and TEM/SAED combined methodologies relevant to analyze cervical dentin submitted to remineralizing nanogels. Thereby, this investigation represents the first attempt to assess the crystal ultrastructure of remineralized cervical dentin, and interpret its morphology. Relative to complementary experimental techniques that ultimately illustrate the clinical outcome of cervical dentin, dark-field TEM (DF-TEM), High Resolution TEM (HRTEM) and Scanning Transmission Electron Microscopy (STEM) should be incorporated into our methodology, for future strategies of research. Nevertheless, our study also has several weakness; application of mechanical loading even exploring some *in vitro* para-functional habits as bruxism, would have expanded the message of this paper, and should have been considered in further research.

Conclusion

Crystallinity increased at cervical dentin treated with Zn-NPs based-gel at 7 d in both 002 and 300 reflections. The scarce randomly oriented and mature crystallites provided both better mechanical properties and long degradation times. These conditions delayed the effects of erosion, as principal etiological factor in dentin hypersensitivity, making dentin more resistant to mechanical and other chemical challenges.

After 7 d, cervical dentin treated with Ca-NPs based-gels showed lower crystallinity than dentin treated with Zn-NPs based-gel, providing more amorphous phase with decreased chemical stability, but higher solubility, biocompatibility and biodegradability. This amorphization became associated to smaller crystallite size with right-defined lineation, and provided an ion-rich environment, favorable for *in situ* dentin remineralization, facilitating the physio-pathological dentin repair process.

The shortest and narrowest crystallite size, and the lowest crystallinity and maturity of minerals were achieved by dentin treated with doxycycline-NPs based-gel after 7 d, thus providing both poor

mechanical performance and chemical stability to the new randomly oriented minerals, discouraging its use to treat dentin hypersensitivity despite its antibacterial and anticollagenolytic activity.

Conflict of interest

The authors (both the corresponding and co-authors) have stated explicitly that there are no conflicts of interest in connection with this article.

Acknowledgements

This work was supported by the Ministry of Economy and Competitiveness (MINECO) and European Regional Development Fund (FEDER) Projects MAT2014-52036-P and MAT2017-85999-P. The authors thank the technical support of PhD Inmaculada Cabello for sample preparation and manuscript edition.

References

Bigi A, Boanini E, Gazzano M, Kojdecki MA, Rubini K (2004) Microstructural investigation of hydroxyapatite-polyelectrolyte composites. *Journal of Materials Chemistry* **14,** 274-279.

Bindu P, Thomas S (2014) Estimation of lattice strain in ZnO nanoparticles: X-ray peak profile analysis. *Journal of Theoretical and Applied Physics* **8**, 123-134.

Bodier-Houllé P, Steuer P, Voegel JC, Cuisinier FJ (1998) First experimental evidence for human dentine crystal formation involving conversion of octacalcium phosphate to hydroxyapatite *Acta Crystallographica. Section D, Biological Crystallography* **54**, 1377-1381.

Chaturvedi R, Gill AS, Sikri P (2008) Evaluation of the regenerative potential of 25% doxycycline-loaded biodegradable membrane vs biodegradable membrane alone in the treatment of human periodontal infrabony defects: a clinical and radiological study. *Indian Journal of Dental Research* **19**, 116-123.

Gajjeraman S, Narayanan K, Hao J, Qin C, George A (2007) Matrix macromolecules in hard tissues control the nucleation and hierarchical assembly of hydroxyapatite. *The Journal of Biological Chemistry* **282**, 1193-1204.

Hanschin RG, Stern WB (1995) X-ray diffraction studies on the lattice perfection of human bone apatite (Crista iliaca). *Bone* **16**, 355S-363S.

Karan K, Yao X, Xu C, Wang Y (2009) Chemical Profile of the Dentin Substrate in Non-Carious Cervical Lesions. *Dental Materials* **25,** 1205-1212.

Landau LD, Lifshit EM (1980) *Statistical Physics (Part 1)*, 3rd edn., Oxford, UK: Butterworth-Heinenann Ltd.

Lee DU, Yun DY, No YS, Hwang JH, Lee CH, Kim TW (2013) Effect of applied voltage on the structural properties of SnO_2 nanostuctures grown on indium-tin-oxide coated glass substrates. *Journal of Nanoscience and Nanotechnology* **13,** 7596-7599.

Liss KD, Bartels A, Schreyer A, Clemens H (2003) High-energy X-rays: a tool for advanced bulk investigations in materials science and physics. *Textures and Microstructures* **35,** 219-252.

Liu Y, Huang J, Li H (2013) Synthesis of hydroxyapatite-reduced graphite oxide nanocomposites for biomedical applications: oriented nucleation and epitaxial growth of hydroxyapatite. *Journal of Materials Chemistry B* **1**, 1826-1834.

Low IM (2004) Depth-profiling of crystal structure, texture, and microhardness in a functionally graded tooth enamel. *Journal of the American Ceramic Society* **87**, 2125-2131.

Medina-Castillo AL, Fernandez-Sanchez JF, Segura-Carretero A, Fernandez-Gutierrez A (2010) Micrometer and submicrometer particles prepared by precipitation polymerization: thermodynamic model and experimental evidence of the relation between flory's parameter and particle size. *Macromolecules* **43,** 5804-5813.

Moshaverinia A, Ansari S, Moshaverinia M, Roohpour N, Darr JA, Rehman I (2008) Effects of incorporation of hydroxyapatite and fluoroapatite nanobioceramics into conventional glass ionomer cements (GIC). *Acta Biomaterialia* **4,** 432-440.

Osorio R, Alfonso-Rodríguez CA, Medina-Castillo AL, Alaminos M, Toledano M (2016b) Bioactive Polymeric Nanoparticles for Periodontal Therapy. *PloS One* **11,** e0166217.

Osorio R, Cabello I, Medina-Castillo AL, Osorio E, Toledano M (2016a) Zinc-modified nanopolymers improve the quality of resin-dentin bonded interfaces. *Clinical Oral Investigations* **20**, 2411-2420.

Perales F, Agullo-Rueda F, Lamela J, De las Heras C (2008) Optical and structural properties of Sb_2S_3/MgF_2 multilayers for laser applications. *Journal of Physics D: Applied Physics* **41**, 045403.

Peumans M, De Munck J, Mine A, Van Meerbeek B (2014) Clinical effectiveness of contemporary adhesives for the restoration of non-carious cervical lesions A systematic review. *Dental Materials* **30**, 1089-1103.

Saeki K, Marshall GW, Gansky SA, Parkinson CR, Marshall SJ (2016) Strontium effects on root dentin tubule occlusion and nanomechanical properties. *Dental Materials* **32,** 240-251.

Toledano M, Aguilera FS, Osorio, Lopez-Lopez MT, Cabello I, Toledano-Osorio M, Osorio R (2016) Submicron-to-nanoscale structure characterization and organization of crystals in dentin bioapatites. *RSC Advances* **6,** 45265-45278.

Toledano M, Osorio R, Osorio E, Medina-Castillo AL, Toledano-Osorio M, Aguilera FS (2017) Ions-modified nanoparticles affect functional remineralization and energy dissipation through the resin-dentin interface. *Journal of the Mechanical Behavior of Biomedical Materials* **68**, 62-79.

Wang F, Guo E, Song E, Zhao P, Liu J (2010) Structure and properties of bone-like-nanohydroxyapatite/gelatin/polyvinyl alcohol composites. *Advances in Bioscience and Biotechnology* **1**, 185-189.

Wang Z, Jiang T, Sauro S *et al.* (2011) The dentine remineralization activity of a desensitizing bioactive glass-containing toothpaste: an in vitro study. *Australian Dental Journal* **56**, 372-381.

Xue J, Zavgorodniy AV, Kennedy BJ, Swain MV, Li W (2013) X-Ray microdiffraction, TEM characterization and texture analysis of human dentin and enamel. *Journal of Microscopy* **251**, 144-153.

Yoshizaki KT, Francisconi-Dos-Rios LF, Sobral MA, Aranha AC, Mendes FM, Scaramucci T (2017) Clinical features and factors associated with non-carious cervical lesions and dentin hypersensitivity. *Journal of Oral Rehabilitation* **44** 112-118.

Zavgorodniy AV, Rohanizadeh R, Swain MV (2008) Ultrastructure of dentine carious lesions. *Archives of Oral Biology* **53,** 124-132.

Zhang Z, Zhou F, Lavernia EJ (2003) On the analysis of grain size in bulk nanocrystalline materials via X-ray diffraction. *Metallurgical and Materials Transactions A* **34,** 1349-1355.

Table 1. Micro-X-ray diffraction pattern analysis approach of dentin surfaces after NPs application.

		002 plane			310 plane			*H/L*
	Storage time	**FWHM**	***H*: Scherrer equation (nm) (τ)**	**R_{hkl}**	**FWHM**	***L*: Scherrer equation (nm) (τ)**	**R_{hkl}**	
Un-treated	24 h	0.0161	9.22	1.044	0.0328	4.70	1.686	2.08
	7 d	0.0167	8.89	1.055	0.0332	4.65	1.740	1.91
NPs	24 h	0.0147	10.12	1.101	0.0323	4.77	1.638	2.12
	7 d	0.0141	10.56	1.599	0.0292	5.27	1.464	2.00
D-NPs	24 h	0.0150	9.92	0.958	0.0335	4.60	1.633	2.16
	7 d	0.0157	9.45	1.102	0.0326	4.73	1.638	2.00
Ca-NPs	24 h	0.0151	9.88	1.102	0.0326	4.73	1.638	2.09
	7 d	0.0144	10.31	1.599	0.0307	5.02	1.464	2.05
Zn-NPs	24 h	0.0144	10.32	1.402	0.0290	5.32	1.508	1.94
	7 d	0.0138	10.82	1.263	0.0300	5.14	1.616	2.11

Abbreviations: NPs: Nanoparticles; FWHM: Full-width half-maximum

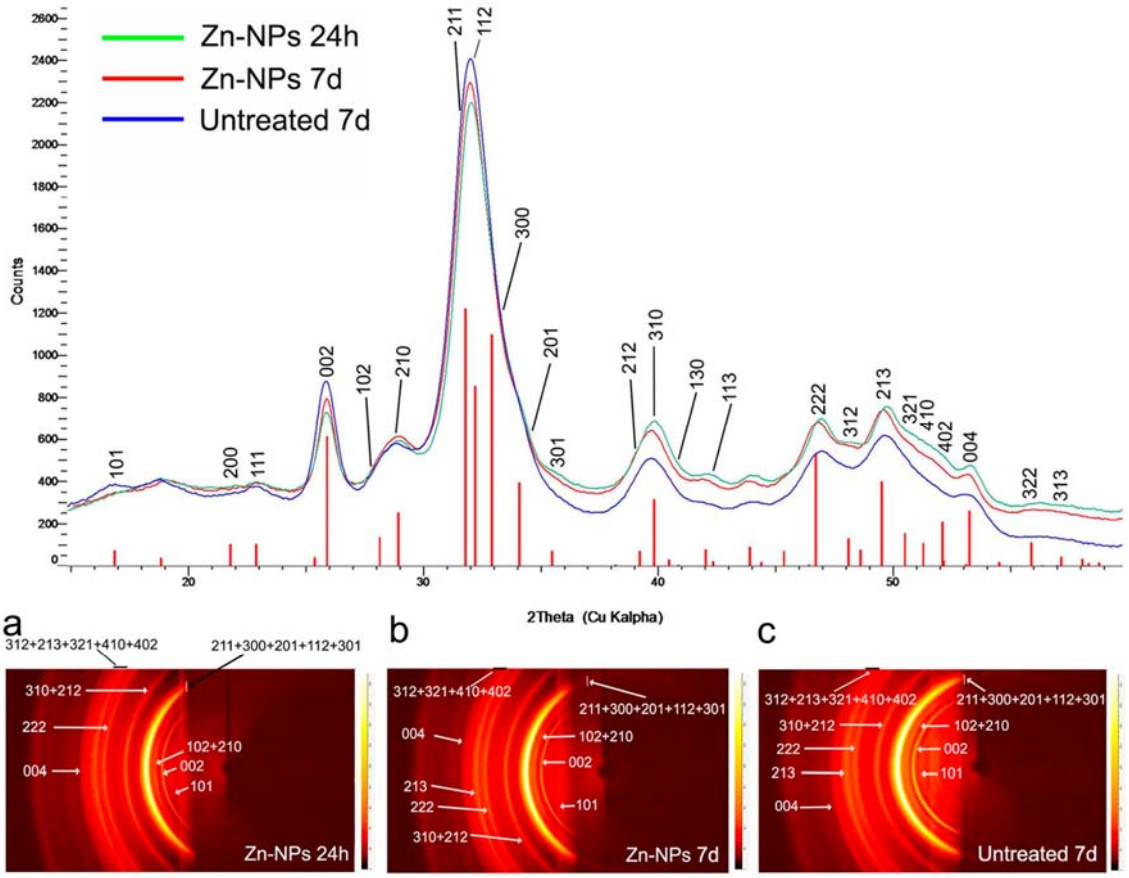

Figure 1. Refined μXRD[2] profiles of cervical dentin treated with Zn-NPs based-gel after 24 h and 7 d of PBS storage. Samples of untreated cervical dentin (untreated) and stored 7 d in PBS have also been analyzed. The corresponding Debye-Scherrer rings are shown in inset a (after 24 h), b (after 7 d) and c (7 d, untreated). Vertical bars represent HAp peaks.

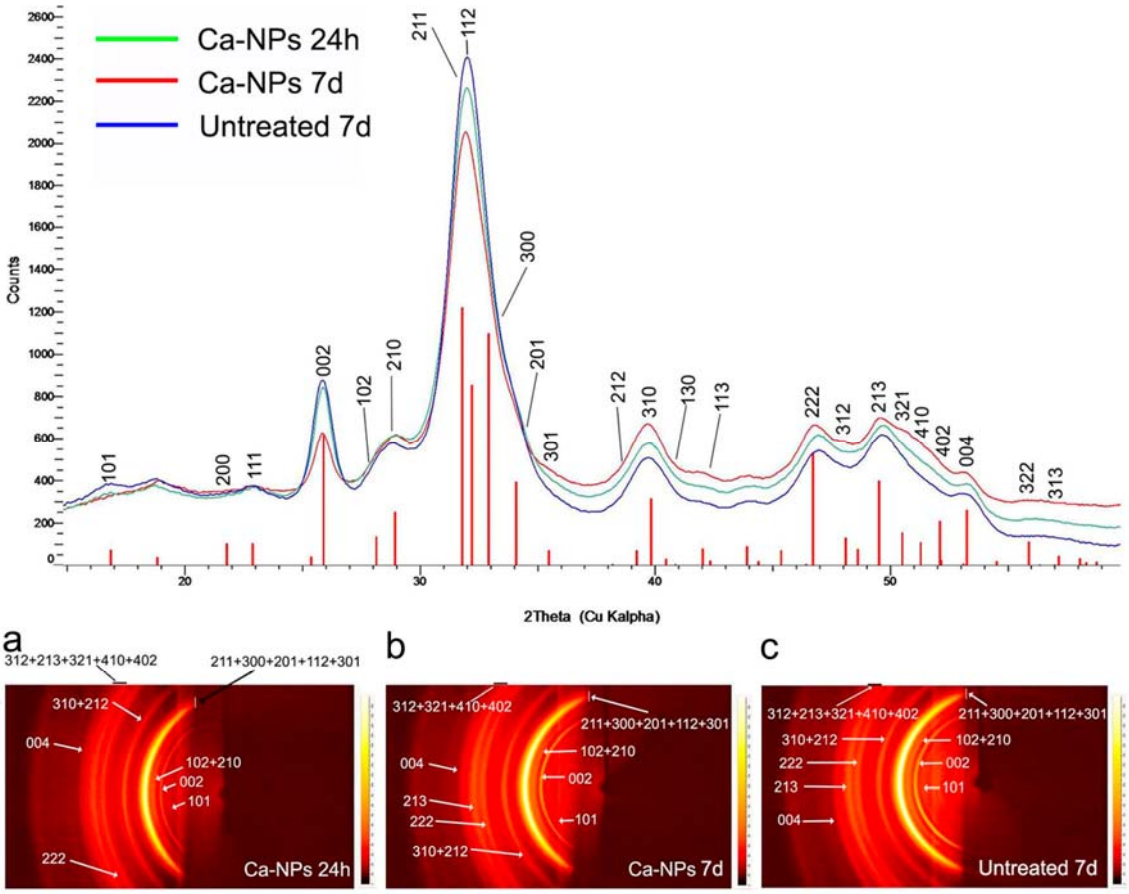

Figure 2. Refined μXRD^2 profiles of cervical dentin treated with Ca-NPs based-gel after 24 h and 7 d of PBS storage. Samples of untreated cervical dentin (untreated) and stored 7 d in PBS have also been analyzed. The corresponding Debye-Scherrer rings are shown in inset a (after 24 h), b (after 7 d) and c (7 d, untreated). Vertical bars represent HAp peaks.

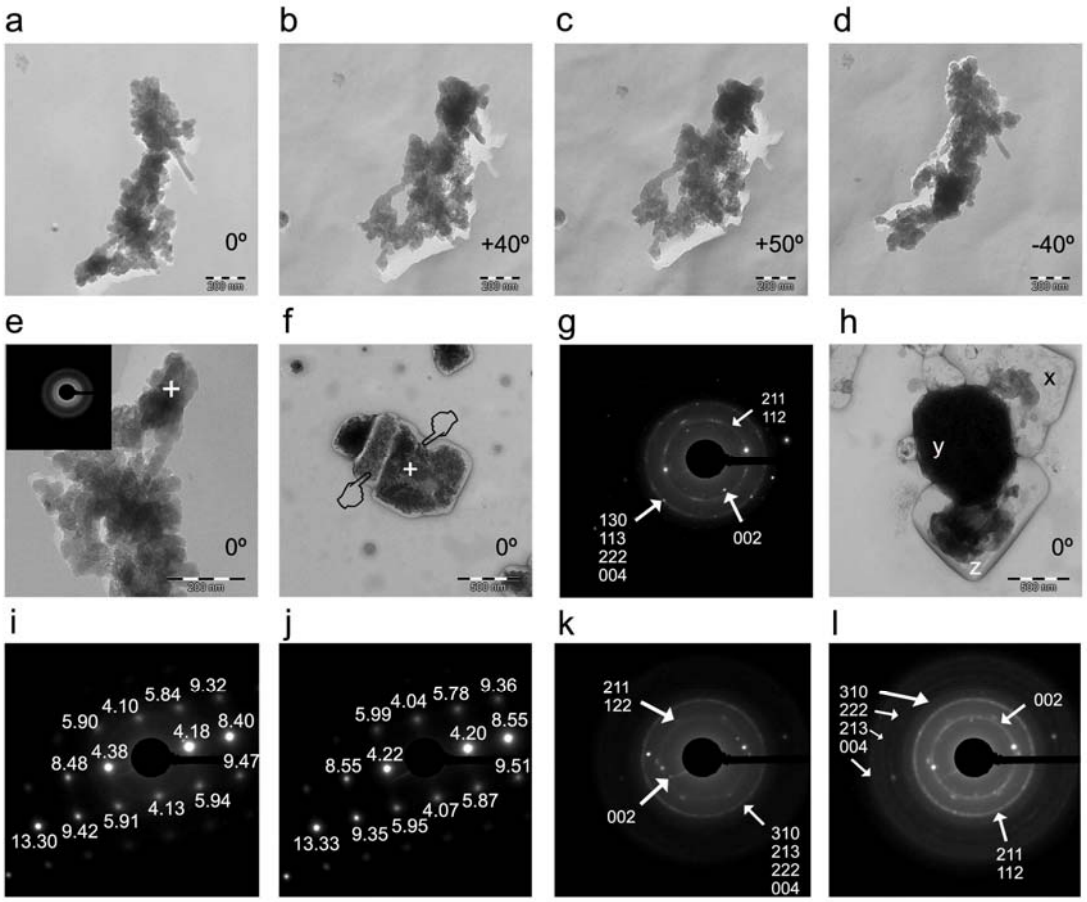

Figure 3. Bright-field of an assembly of polyhedral apatite crystals of cervical dentin treated with Zn-NPs based-gel, 7 d storage. Views at different tilt angles after tomographic reconstructions are presented at 0º (a), 40º(b), 50º(c), and -40º (d) (scale bars: 200 nm). (e), Magnified observation of a section from (a), showing the in detailed polyhedral apatite appearance of crystallites (scale bar: 200 nm). A selected area electron diffraction (SAED) of the crystal (+) shown in (a), at nanoscale. (f), Bright-field of a three-phase staggered order block-like crystallites of cervical dentin treated with Zn-NPs based-gel, 7 d storage (scale bar: 500 nm). The pointers mark the cut domains with the sectioned crystals seen face-on. (g), selected area electron diffraction (SAED) of the crystal (+) shown in (f), at nanoscale, showing the labeled lattice planes of hydroxyapatite crystals; it exhibits the sharp 002 diffraction peak reflecting the elongated nature of the crystals, a first broad diffraction band containing 211 and 112 grouped peaks, and a second broad diffraction band containing 130, 113, 222, and 004 peaks. Note that the spots are more clearly delineated in this pattern, as compared to those obtained in a, supporting the larger crystal size. (h), Bright-field of a rounded/drop-like or plate-like shaped crystal of cervical dentin treated with Zn-NPs based-gel, 7 d storage (scale bar: 500 nm. (i) and (j), selected area electron diffractions (SAED) of the crystal (+) shown in h, points ”y” and “z”, respectively, at nanoscale. Diffraction pattern containing diffuse halo rings only, indicating some amorphous structure and clear *d* spacing values, meaning the presence of remnant crystallite matter. Both figures represent zone axis patterns in which the matrix reflections are intense, faint additional reflections are also visible (arrowheads). The presence of crystals less than micron size (nm-1) is provided. k and l, selected area electron diffractions (SAED) of the crystal (+) shown in h, points “z” and “x”, respectively, at nanoscale.

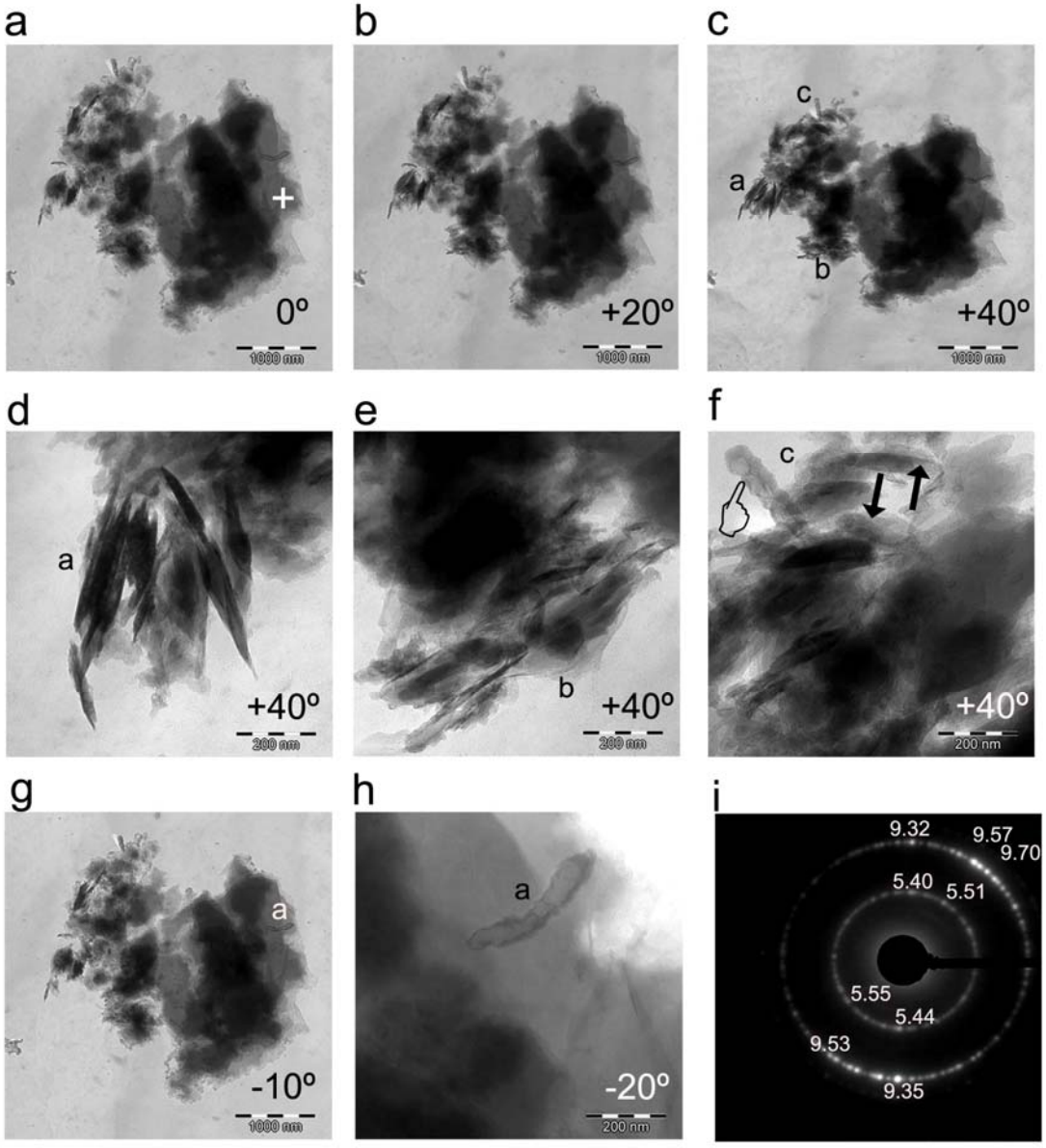

Figure 4. Bright-field of an assembly of polymorphic apatite crystals of cervical dentin treated with Ca-NPs gel-based, after 7 d storage. Views at different tilt angles after tomography reconstructions are presented at: 0º(a), 20º(b), 40º(c), -10º(g) (scale bars: 1000 nm). (d), (e), Magnified observation of a section from (c), showing the in detailed strong needle-like apatite crystallites. Both images reveal that the particles have multiple domains of locally aligned crystal arrays (scale bars: 200 nm). (f), magnified observation of a section from (c), showing the in detailed polyhedral and cubic (pointer) or needle-like (arrows) apatite appearance of crystallites (scale bar: 200 nm). (h), magnified observation of a section from (g), showing the staggered order of polygon crystallites (scale bar: 200 nm). (i), selected area electron diffraction (SAED) of the crystals (+) shown in (a) at microscale; it exhibits clear halo rings and diffraction d spacing values of submicron size crystals (nm-1), indicating the presence of crystalline matter, whose pattern shows relatively uniform reflections for all variants. It also confirms the presence of hexagonal apatite and a highly polycrystalline structure.

Supporting Information

Additional Supporting Information may be found in the online version of this article:

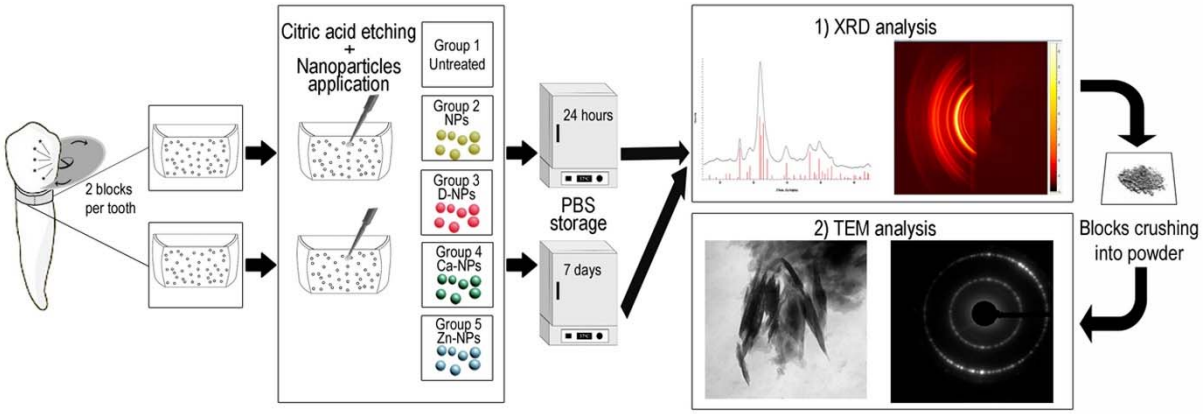

Figure S1. Graphical abstract illustrating the procedure to obtain the cervical dentin blocks submitted to the exposed experimental methodology.

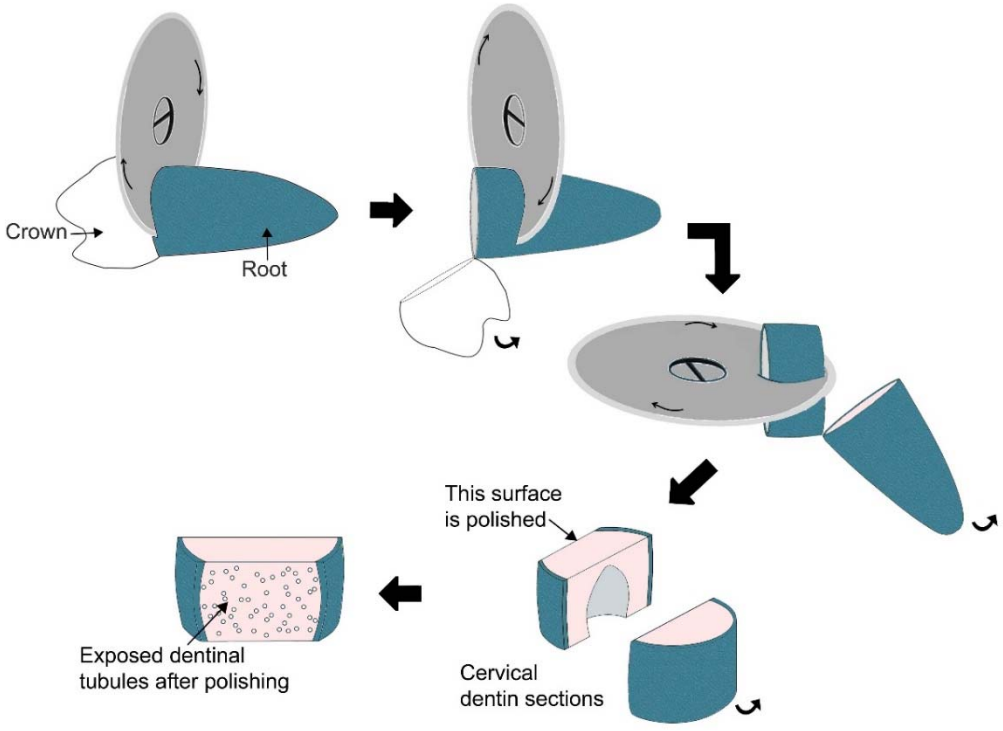

Figure S2. Schematic representation of specimen preparation. Tooth coronal section was discarded (1), a longitudinal cut was also made to obtain two halves of the original specimen (2), two dentin blocks were prepared by cutting below the cement-dentinal junction (3), surfaces were polished (4) to expose the cervical dentin.

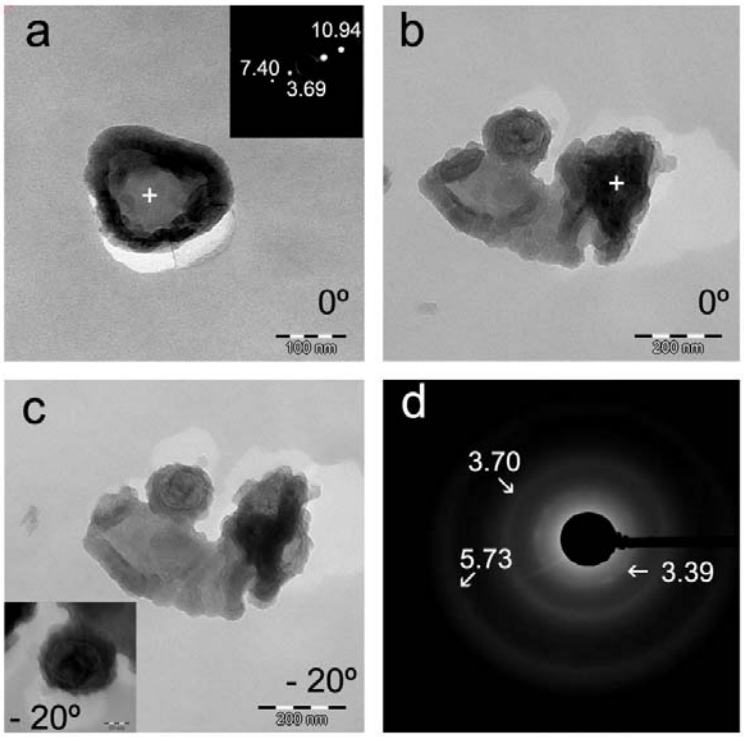

Figure S3. (a), Bright-field of an assembly of block-like or rounded apatite crystals of cervical dentin treated with D-NPs based-gel, after 7 d storage. At the image is observed that the particle has a domain of locally aligned crystal arrays (scale bar: 100 nm). An inset (top right) which corresponds to a selected area electron diffraction (SAED) d-values of micron and submicron size (+) is also shown. (b) and (c), Bright-field of an assembly of polymorphic apatite crystals of cervical dentin treated with un-doped NPs based-gel, after 7 d storage, at 0º and -20º tilted angles, respectively (scale bars: 200 nm). (c), high magnification of a section at the apatite crystal which confirms the overlapped order of the polycrystalline structure. (d), selected area electron diffraction (SAED) pattern of the crystals (+) shown in (B), at nanoscale. Diffractography depicts diffuse halo rings and d spacing values of submicron size crystals.

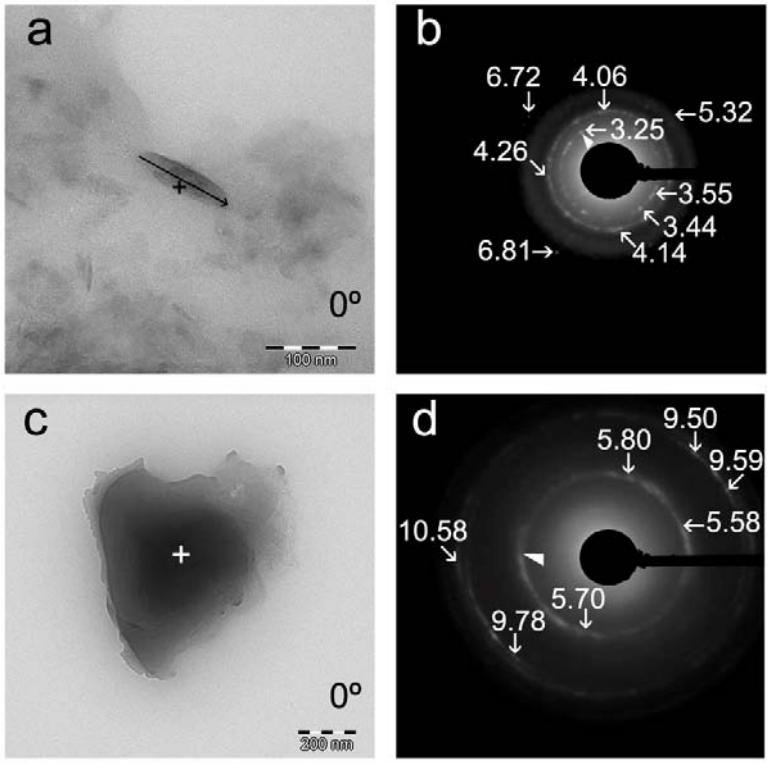

Figure S4. (a), Bright-field of an assembly of needle-like apatite crystals of untreated cervical dentin, 24 h storage (scale bar: 100 nm). The arrow points the predominant direction of the c-axes. (c), Bright-field of an assembly of platelet elongated and agglomerated crystals in the c-direction of untreated cervical dentin, after 7 d storage. The particle has not domain of locally aligned crystal arrays (scale bar: 200 nm). (b) and (d), selected area electron diffractions (SAED) of the crystal (+) shown in a and c, respectively, at nanoscale. (b), almost no preferred orientation is observed, meanwhile at (d) orientation is detected (arrowheads). They depict diffraction pattern containing diffuse halo rings only, indicating some amorphous structure and the interplanar spacing values, indicating the presence of remnant crystallite matter. They also provide the presence of crystals less than micron size (nm-1).